Real-Time Reconfiguration-Based All-Cell Flexibility and Capacity Maximum Utilization of Second- Life Batteries

Article *in* IEEE Transactions on Transportation Electrification · February 2025

DOI: 10.1109/TTE.2024.3399218

Zhongbao Wei
Beiijng Institute of Technology

Xinghua Liu
Xi'an University of Technology

Yang Li
Chalmers University of Technology

Rui Wang
Northeastern University

Real-time Reconfiguration-Based All-Cell Flexibility and Capacity Maximum Utilization of Second-Life Batteries

Zhongbao Wei, *Senior Member*, *IEEE*, Haoyong Cui, Xinghua Liu, *Senior Member*, *IEEE*, Yang Li, *Senior Member*, *IEEE*, Rui Wang, *Member*, *IEEE*

***Abstract*—The capacity underutilization caused by cell inconsistency hinders the efficient utilization of lithium-ion battery packs. This is particularly critical for the second-life battery utilization where high cell inconsistency exists. To address this issue, this paper proposes a multi-scale reconfiguration control method enabled by an efficient reconfigurable battery topology, aiming to maximize the pack's capacity utilization. In this regard, a novel 4-switch reconfigurable battery topology is proposed, offering the advantages of all-cell flexibility and reasonable complexity. Building upon this, an all-cell equalization method is proposed, combining intra-module current sharing and three forms of inter-module energy distribution to achieve maximum pack capacity utilization. Moreover, real-time reconfiguration ensures effective charge transmission when the pack voltage deviates from the expected threshold. A lab-scale prototype of the reconfigurable battery pack is tested, and experimental results confirm that the proposed design and reconfiguration control can improve pack capacity utilization and efficiency by 10.96% and 14.34%, respectively, without any redundant design. This method provides a feasible solution for grouping and system management of second-life battery systems consisting of highly inconsistent cells.**

***Index Terms*—All-cell flexibility, maximum capacity utilization, reconfigurable battery, voltage stabilization.**

I. INTRODUCTION

LITHIUM-ION batteries (LIBs) have gained widespread use in electric vehicles (EVs) due to their high energy/power density and long lifespan[1-4]. In EV applications, the first life of LIBs typically ends when any cell within the pack experiences a 20% capacity drop, ensuring expected mileage and reliability [5]. Consequently, retired batteries retain significant residual capacities that can be repurposed for a second life, such as grid energy storage. It has been projected that by 2035, the number of post-vehicle battery packs available for second-life use could reach 6.8 million, and the second-life battery business could grow from $16 million in 2014 to $3 billion [6]. Given this substantial market potential, efficient second-life utilization becomes highly significant.

The capacities of second-life batteries can vary greatly due to their diverse operating histories. Since the pack's available capacity is determined by the weakest cell, the performance of the pack deteriorates significantly as the inconsistency spreads. Additionally, the pack voltage fluctuates during charge and discharge cycles, leading to an uncontrollable voltage gap at the pack-load level and reducing charge transmission efficiency [7]. Both of these factors contribute to an irreversible drop in efficiency, resulting in significantly higher user-end costs.

Passive and active balancing methods are commonly used to address cell inconsistency [8]. Passive balancing dissipates excess charge from higher capacity cells through resistors, but this approach is undesirable due to its thermal energy losses and lower energy efficiency [9]. Active balancing, on the other hand, relies on conversion elements [10] for directional charge transfer [11], but it is plagued by high costs, limited balancing speed, and challenging layout requirements [12]. In terms of the pack-load voltage gap issue, voltage compensation is often achieved using DC/DC converters [13]. Centrally controlled DC/DC converters are high-power devices placed at the pack terminal to maintain voltage, while low-power DC/DC converters are distributed in series [14] or in parallel [15] with cells/modules to regulate local voltages and ensure pack voltage stability. Although effective for voltage compensation, the implementation of DC/DCs is associated with space limitations and efficiency losses, especially in large pack-load voltage gap.

Reconfigurable battery systems have emerged as a promising direction recently, reflecting the future trend of smart battery management [16]. With adaptive configuration switching, reconfigurable batteries offer solutions for battery optimization in various applications, including efficient equalization [17], extended lifespan [18], and voltage stabilization [19]. Among the limited studies in this area, offline optimization-based reconfiguration approaches stand out due to guaranteed optimality in capacity utilization. These methods employ optimization algorithms such as dynamic programming (DP) to determine the optimal cell combination that maximizes pack capacity [20],

This work is supported by the National Key Research and Development Program of China under Grant 2023YFB2407900, National Natural Science Foundation of China under Grant U22A20227 and 52072038. *(Corresponding author: Zhongbao Wei)*

Z. Wei and H. Cui are with the National Engineering Research Center of Electric Vehicles, School of Mechanical Engineering, Beijing Insti-tute of Technology, Beijing 100081, China (e-mail: weizb@bit.edu.cn; cuihy@bit.edu.cn).

X. Liu is with the School of Electrical Engineering, Xi'an University of Technology, China (liuxh@xaut.edu.cn).

Y. Li is with the Department of Electrical Engineering, Chalmers University of Technology (email: yang.li@ieee.org).

R. Wang is with the College of Information Science and Engineering, Northeastern University, Shenyang, China (email: wangrui@ise.neu.edu.cn).

identify optimal reconfiguration operation for cell balancing [21], or optimize the configuration for minimal state of charge (SOC) consumption [22]. Despite guaranteed optimality, these methods rely on the assumption of a given load, which is often not met in practical applications.

Compared to offline optimization, real-time reconfiguration is more appropriate for real-world applications as it determines switching actions based on online detection of battery status. Although still in its early stages, real-time reconfiguration has been utilized for cell equalization. This is achieved by bypassing the weakest cell in a timely manner, as demonstrated in [23, 24], to address the capacity inconsistency in the battery pack. However, the weak-cell isolation always requires the presence of a redundant cell to compensate for the resulting vacancy.

Reconfiguration also enables the pack voltage stabilization to alleviate the excessive variation of pack voltage. To compensate for the voltage deficit resulting from declining SOC, redundant cells are introduced into the system [19]. Alternatively, an adaptive approach determines the optimal number of modules to maintain a constant pack voltage [25]. However, the inclusion of redundant cells/modules unavoidably leads to a decrease in cell utilization rate and the accelerated degradation of frequently-used cells [26].

It can be concluded that existing reconfiguration methods have several explicit drawbacks. First, these methods treat modules as inseparable entities for optimization, preventing any cell-level manipulation. This limits the flexibility of reconfiguration and hinders optimized battery utilization. Second, existing works only consider simple pack topologies and have not explored efficient solutions for more practical and complex parallel-series topologies. Third, the inclusion of redundant cells/modules in the reconfiguration process increases the complexity and cost of the battery system. Currently, there is a lack of efficient solutions that exploit the potential of configuration itself without introducing any auxiliary components.

To bridge the aforementioned gaps, this paper proposes a novel multi-scale reconfiguration control method. This method is based on a 4-switch reconfigurable battery topology, aiming to achieve all-cell flexibility, consistency, and output voltage stabilization. The following primary contributions are made: (1) With the intra- and inter-module adaptive energy allocation on a novel 4-switch battery topology, the highly-desired all-cell flexibility and equalization can be realized for the practical series-parallel battery pack. (2) The reconfiguration contributes to exploiting the pack capacity to the greatest extent even with high cell in-consistency in the second-life battery utilization. The pack capacity utilization rate can be improved by 10.96%. (3) The reconfiguration can also stabilize the pack voltage within an expected range to ensure high conversion efficiency. (4) The capacity maximum utilization and voltage stabilization can be achieved without module replacement or redundant design, which reduces the system cost greatly.

The rest of the paper is organized as follows. Section II introduces the proposed reconfigurable battery topology and experimental setup for validation. Section III elaborates the multi-scale reconfiguration control method. Section IV presents the experimental results and discussions. Section V draws the primary conclusions of the paper.

II. Reconfigurable Topology

A. Reconfigurable Battery Topology and Prototype

To meet the practical demands for output power and voltage, LIB cells are typically connected in series and parallel to form a battery pack. However, it should be highlighted that the static connections in traditional packs do not fully utilize the cell capacities, particularly in the context of high cell inconsistency observed during the second-life usage of LIBs.

Unlike traditional batteries, reconfigurable batteries possess a distinctive feature where cells are equipped with switches, enabling flexible reconstruction [27]. A novel 4-switch reconfigurable topology is employed to strike a favorable balance between complexity and flexibility, as shown in Fig. 1a.

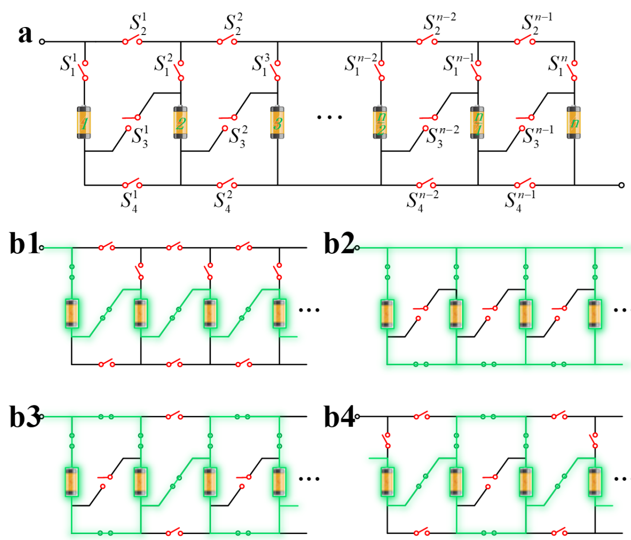

Fig. 1. 4-switch reconfigurable battery. a) Schematic diagram of 4-switch reconfigurable battery. b) Allowing connection of the 4-switch reconfigurable battery: series connection in b1), parallel connection in b2), parallel-series connection (cells are connected in parallel first and then connected in series to constitute a pack) in b3), and arbitrary combination of connection in b4).

The 4-switch topology enables various combinations of series, parallel, and parallel-series connections among cells, as shown in Fig. 1b. The inclusion of switch S_1^k (k is the number of cells) grants independence to each cell, regardless the cell connection. Additionally, switches S_2^k, S_3^k, and S_4^k allow for dynamic switching between series and parallel connections of cells/modules. The high reconfigurability yet moderate number of switches endow the 4-switch topology with board application prospects and potentials for various performance optimization of battery pack. For example, this topology allows regular calibration of all in-pack cell capacity, promising the robustness of reconfigurable algorithms in the presence of capacity changes induced by temperature fluctuations and battery degradation.

B. Prototype of Reconfigurable Battery Pack

A laboratory-scale prototype with assembly flexibility is es-

This article has been accepted for publication in IEEE Transactions on Transportation Electrification. This is the author's version which has not been fully edited and content may change prior to final publication. Citation information: DOI 10.1109/TTE.2024.3399218

tablished, as depicted in Fig. 2. The prototype comprises a battery management system (BMS), a reconfigurable battery pack consisting of $LiFePO_4$ cells and switch arrays, as well as a DC/DC converter for voltage conversion. The capacities of employed cell are distributed within [1.4Ah, 2Ah], reflecting a high capacity inconsistency typical observed in second-life LIBs. The BMS (Huahai Technologies, RapidECU-U4B) estimates the cell status based on current and voltage data collected by sensors. It then makes real-time decisions on the switching actions and sends the corresponding commands to the switch array for dynamic adjustment of the cell connections. The DC/DC converter operates to compensate for voltage gaps resulting from changes in battery equilibrium potential and overpotential. All the components used in the reconfigurable prototype are off-the-shelf, widely adopted parts, enabling it to operate in real-world scenarios rather than being limited to controlled laboratory environments.

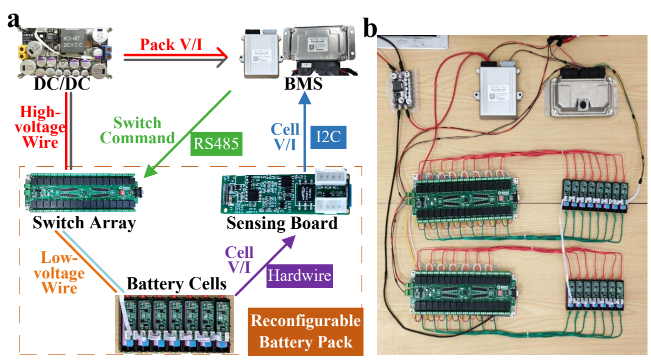

Fig. 2. Lab-scale prototype of 4-switch reconfigurable battery pack: (a) device connection and communication, and (b) device layout.

III. Multi-scale Reconfiguration Control

Based on the designed battery prototype, a multi-scale control method is proposed for capacity maximum utilization and voltage stabilization. To maximize the pack's capacity, a hierarchical equalization control method is employed, which is further divided into intra- and inter-module equalization.

A. Intra-module Cell Equalization

Parallel-cell imbalances are common within module, which is reflected in the following three aspects: (1) More than 10% SOC deviation is observed when two intra-module cells with the same initial SOC but different capacities are discharged at 1C [28]. (2) Intra-module imbalance worsens as the discharging current increases [29]. (3) Spontaneous intra-module equalization is only notable when the cells are idle, requiring nearly 1 hour for the equalization of 4 cells [30]. These findings highlight the need for improving intra-module cell equalization.

The key of intra-module equalization is to distribute the current flux among parallel cells in a manner that ensures equalization. To achieve this, an intra-module cell equalization method is proposed. The procedure of the intra-module cell equalization is summarized in Table I. The core idea of intra-module cell equalization is to differentiate the cell conduction time based on its capacity ownership and consumption rate. In specific implementation, the conduction duration of the intra-module cells is regulated by intermittently PWM engagement of the cell series switch S_1^k. Due to the mutual backup of parallel cells, the failure or removal of any individual cell will not adversely affect the regular functioning of the other cells.

It should be noted that the OFF duration of each intra-module cell is staggered to ensure that at least one cell remains online to sustain the main-circuit current, as the module will be offline if the bypass period of parallel cells within the module overlaps. Moreover, the PWM period should be set within a reasonable range. This is because high-frequency PWM results in remarkable energy loss, while low-frequency PWM compromises the control resolution and, the equalization performance.

TABLE I
Procedure of the intra-module cell equalization method.

Input: Capacity $C_n^k(0)(T)$, ohmic and polarization resistances $R_s^k(T)$, $R_{p1}^k(T)$, $R_{p2}^k(T)$ of the *k*-th cell ($k \in [1, K]$[a)]) at current temperature.

Step 1: Initial duty cycle calculation: Set $j = 0$[b)], define a proper PWM period, set the initial duty cycle of the maximum-capacity cell $D_k^m(0)$ as 100%, calculate the initial duty cycle of remaining cells $D_k(0)$ as:

$$D_k(0) = D_k^m(0) \cdot \frac{C_n^k(0)(T)}{C_n^m(0)(T)} \cdot \frac{R_s^k(T) + R_{p1}^k(T) + R_{p2}^k(T)}{R_s^m(T) + R_{p1}^m(T) + R_{p2}^m(T)}$$

Step 2: Determination of initial ON/OFF duration of switches: ON duration of each cell is determined by $D_k(0)$ and the PWM period. Stagger each cell OFF duration.

Step 3: Switch actuation:

Cell time-sharing intervention according to the determined ON-OFF duration by intermittently PWM engaging the cell series switch S_1^k; Estimate $SOC_k(j)$ when PWM cycle ends.

Step 4: State feedback:

If $SOC_k(j) < SOC_{thr}$[c)]

Equalization ends;

Else

$j = j + 1$; Fine-tune $D_k(j)$ with cell SOC differences by PID;

Back to Step 3.

[a)] K is the number of cells within a module; [b)] j is the PWM cycle index; [c)] SOC_{thr} is the equalization threshold of SOC.

B. Inter-module Equalization

Unlike existing works that disable the flexibility of intra-module cells, an inter-module equalization controller that involves the participation of all cells is proposed. The inter-module equalization is categorized into three independent modes: cell-transfer, collaborative splitting, and strong-module splitting equalization. These modes are suitable for different adjacent scenarios, including strong-weak, strong-strong, and strong-equalized module adjacency. It should be noted that these three modes cover all possible conditions that may occur during the entire period in equalization.

TABLE II
Procedure of the cell-transfer equalization method.

***Step 1*: (Cell transfer)**

Check all the cell and module capacities at current temperature.

If strong-weak module adjacency is satisfied

The strong-module cell adjacent to the weak module is split out and integrated to the weak.

***Step 2*: (Differentiated discharge)**

The transferred cell undertakes a $1/N$[a] discharge pressure of the weak module. The discharge rate of the weak/strong module is decreased/increased.

***Step 3*: (Cell return)**

If extra capacity of the strong module is released Or lacking capacity of the weak is made up

The transferred cell returns to the strong module.

[a] N is the number of cells in the weak module after cell transfer.

TABLE III
Procedure of the collaborative-splitting equalization method.

***Step 1*: (Collaborative splitting and weak modules exit)**

Check all the cell and module capacities at current temperature.

If strong-strong module adjacency is satisfied

The last/first one-third cells of the former/latter strong module are split out; All split-out cells are combined as a new interim module; A weak module is bypassed.

***Step 2*: (High-rate discharge)**

The two split modules undertake 1.5× high-rate discharge compared with other modules. The bypassed weak module is idle.

***Step 3*: (Dual-module recombination and weak modules return)**

If extra capacity of either strong module is released

The temporary interim module is split to recombine the original two modules; The bypassed weak module re-enters the series module sequence.

TABLE IV
Procedure of the strong-module splitting equalization method.

***Step 1*: (Strong-module splitting and weak modules exit)**

Check all the cell and module capacities at current temperature.

The maximum-capacity cell in the strong module is split out;

The split-out cells and remaining cells constructs two series sub-modules respectively;

A weak module is bypassed to maintain the number of modules.

***Step 2*: (Double-rate discharge)**

The split module undertakes double-rate discharge compared with other modules. The bypassed weak module is idle.

***Step 3*: (Strong-module recombination and weak modules return)**

If extra capacity of the strong module is released

The two sub-modules recombine the original one module; The bypassed weak module re-enters the series module sequence.

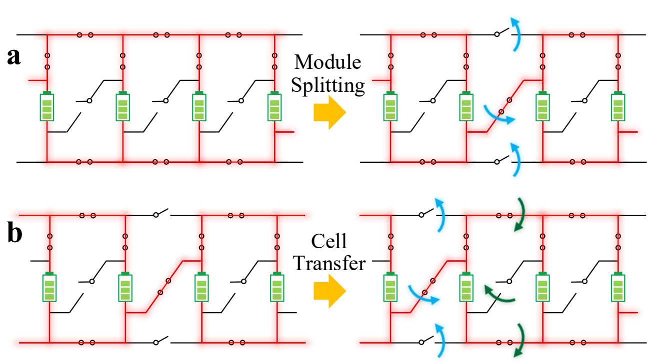

Fig. 3. Switch action of a) module splitting and b) cell-transfer reconfiguration in inter-module equalization.

The procedure for cell-transfer, collaborative splitting and strong-module splitting methods are summarized in Table II, III and IV respectively. These three inter-module reconfigurable equalization methods involve two forms of configuration switching: strong module splitting and cell transfer. The corresponding switching actions are shown in Fig. 3. It can be seen that the module split reconfiguration is realized by the simultaneous actuation of three switches, while the cell transfer reconfiguration requires the coordinated control of six switches.

The three inter-module equalization methods are distinguished by their speed of equalization and aging stress. For instance, the strong-module splitting achieves faster equalization compared to the other two. However, this improved rapidity comes at the cost of increased degradation, as the split-out cells in the strong-module splitting method are exposed to module-level current and may experience premature aging. A comparison of three equalization methods is provided in TABLE V.

TABLE V
Comparison of three forms of inter-module equalization.

Method	Adjacent scenario	Equalizing speed	Battery aging	Complexity
Cell transfer	Strong-weak	Medium	Medium	Low
Collaborative splitting	Strong-strong	Slow	Slow	High
Strong-module splitting	Strong-equalized	Fast	Fast	Medium

It is important to highlight that a wide variation in pack voltage negatively affects energy conversion efficiency. An intuitive approach is to dynamically adjust the number of series modules to keep the total voltage within a narrow range. When the pack voltage falls below the lower threshold in discharge, two strong adjacent modules are reconfigured to form three series modules based on the collaborative splitting principle. Collaborative splitting is chosen for voltage stabilization because it mitigates the degradation tendency of a single split module. Above measures can also be employed for fault-tolerant control of module failures. When a module fails, the collaborative-splitting reconfiguration allows for the compensation of module vacancies arising from the failed module, thereby ensuring the maintenance of a relatively stable pack voltage.

C. Method Overview

The cell-level reconfiguration focuses on intra-module cell equalization control, the module-level reconfiguration is aimed for inter-module equalization control, while the pack-level reconfiguration is oriented towards the pack-voltage stability control. The above three levels of reconfiguration control cooperate with each other to create a multi-scale reconfigurable control method, as illustrated in Fig. 4a.

It worth noting that the proposed multi-scale reconfigurable control method exhibits both hierarchical attributes in logic and a stepwise feature in the time domain. Specifically, the inter-module equalization is prioritized as it requires sufficient capacity margin on cells, which may not be feasible at the later stage of equalization. Once the capacity difference of modules is completely eliminated, intra-module cell equalization begins. When the pack terminal voltage drops below the set threshold during inter- or intra-module equalization, the reconfigurable voltage stability control is triggered to split strong modules in order to maintain a stable pack voltage. The module splitting operation interrupts the original equalizing process and the controller recalculates new equalization objectives for modules and intra-module cells, initiating a new round of equalization starting with inter-module and then intra-module equalization steps.

The aforementioned mechanism of updating equalization targets also applies to fault-tolerant equalization for cell and module failures. If a cell or module fails, the capacity distribution of intra-module cells and the capacity comparison of modules change, rendering the original equalization goal unattainable. To address this, the multi-scale controller adjusts the capacity difference between modules and the PWM duty cycle of cells to achieve equalization in the presence of cell/module faults.

The prioritization of three inter-module equalization methods at different stages of module equalization is shown in Fig. 4b. The combination of cell-transfer and collaborative splitting is recommended in the initial stage of equalization, as it enables rapid equalization while preventing accelerated battery aging. In subsequent stages, when only a few un-equalized modules are adjacent, the independent use of cell-transfer or collaborative splitting is preferred. Once no adjacent un-equalized modules, strong-module splitting is employed to achieve rapid equalization across all modules.

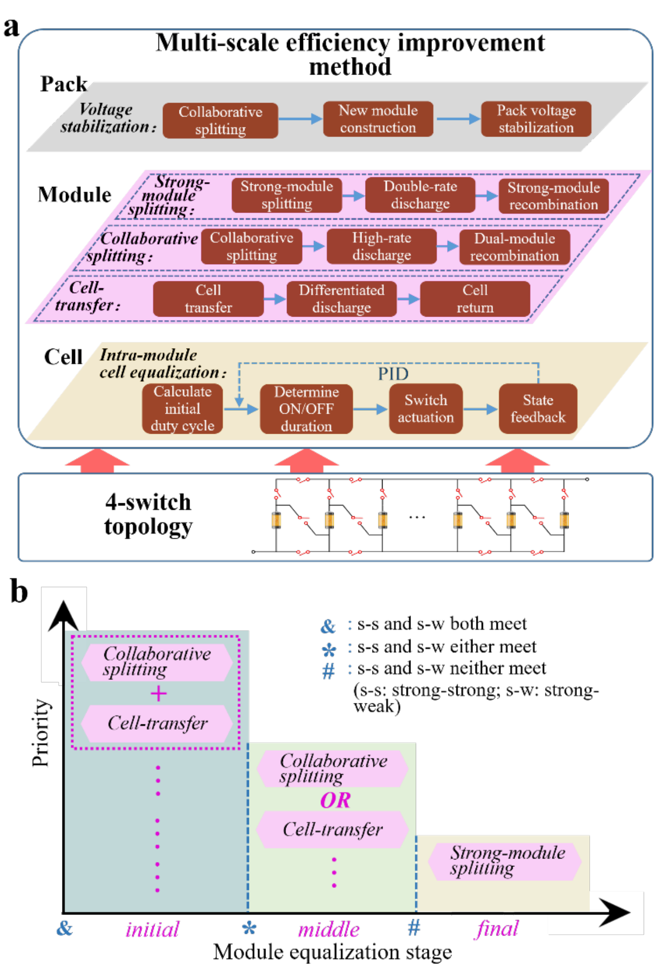

Fig. 4. Schematic diagram of a) multi-scale reconfiguration control method, and b) priority of three inter-module equalization methods.

IV. Results and Discussion

A. Validation of Intra-module Cell Equalization

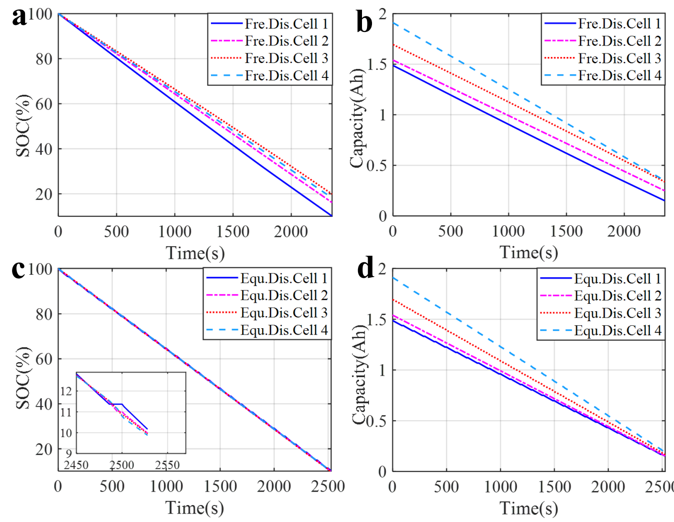

Fig. 5. Intra-module cell dynamics: a) SOC, b) capacity of cells in free discharge, and c) SOC, d) capacity of cells in equalizing discharge.

To validate the effectiveness of intra-module cell equalization, a module with 4 parallel cells is tested. The spontaneous imbalance during free discharge is first investigated. The evolutions of cell SOCs and capacities in free discharge are presented in Fig. 5a and 5b, respectively. It is evident that the cell SOCs deviate from each other as the discharge progresses, resulting in a 10% SOC deviation. This SOC divergence indicates a gradual deterioration of cell imbalance. The initial capacity gaps among cells remain largely unchanged, as the spontaneous allocation of discharge current within the module does not match the capacity distribution among cells.

In contrast, the usage of intra-module equalization leads to a consistent SOC trajectory and gradual convergence of capacity, as depicted in Fig. 5c and 5d. This is attributed to the adaptive charge flux distribution enabled by the equalization method, which ensures consistent SOC consumption irrespective of initial capacity imbalances among cells. Specifically, the capacities of intra-module cells change proportionally with their capacity comparison, aiming to reach an almost common capacity termination. It is observed that all cells almost simultaneously reach the cut-off threshold, with SOC divergence limited to only ±1%, as illustrated in the zoom-in figure in Fig. 5c. This confirms the efficacy of the intra-module equalization approach. Although it seems consume the entire experimental duration to reach equal cell capacity from the perspective of capacity balancing, the goal of intra-module equalization is to balance cell SOCs. The presence of overlapping SOC evolution throughout the experiment demonstrates that the intra-module cells maintain equalization from start to finish.

B. Validation of Inter-module Equalization

To evaluate the performance of inter-module equalization, the intra-module equalization is excluded herein, thus the parallel cells keep free discharge throughout the following three experiments for the validation of inter-module equalization.

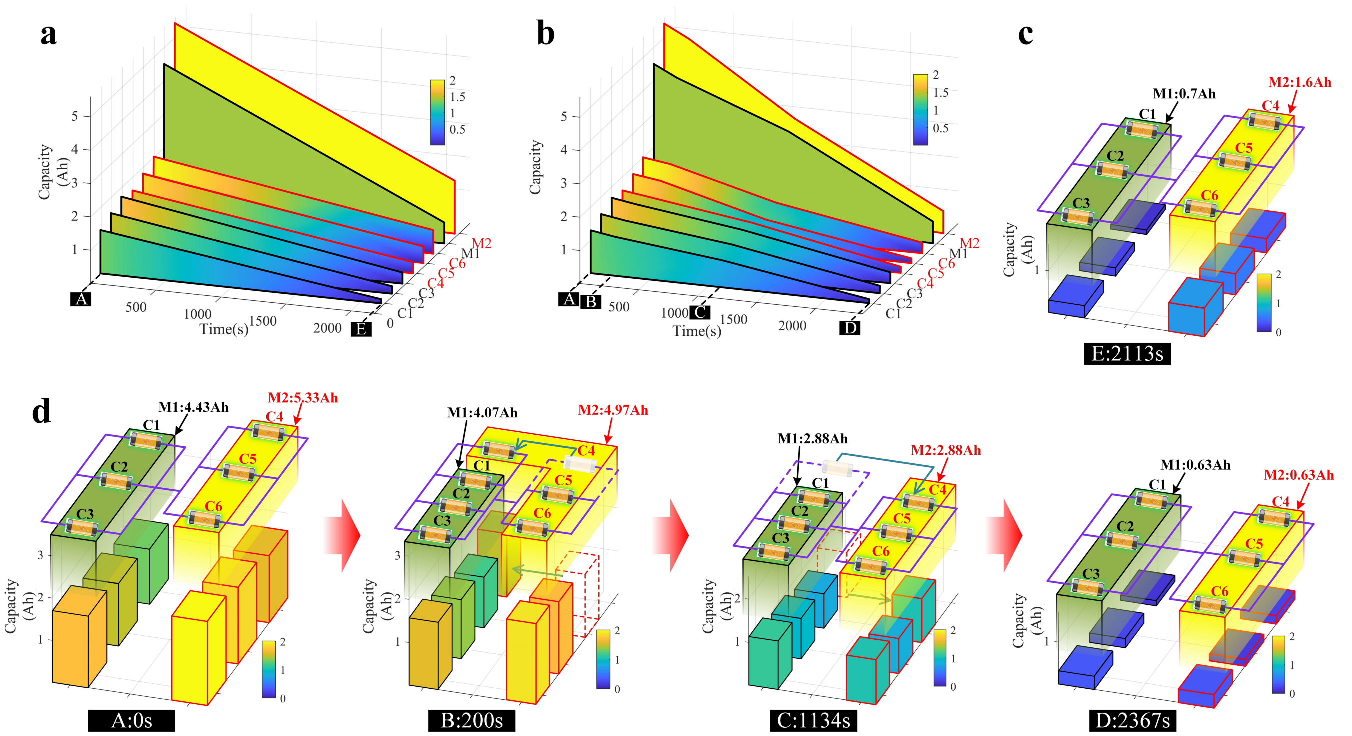

Fig. 6. Capacity of cells and modules: a) without, and b) with the cell-transfer equalization, where the color gradient indicates the amount of cell residual capacity with discharge. c) Module capacity and intra-module cell capacity at the end of non-equalized discharge. d) The cell-transfer equalization process interpreted by configuration switching actions in 4 stages: *A* is the start of discharge, *B* is the cell-transfer stage, *C* represents the cell-return stage, and *D* is the end of equalization.

1) Cell-transfer Equalization:

Cell-transfer equalization is applicable when a strong module is adjacent to a weak module, which is typically encountered during the initial stages of equalization. In this approach, the cell within the strong module that is closest to the weak module is isolated and merged to the weak module. This cell transfer the results in a reduction of current flux across the weak module, while increasing the current flux across the strong module. Consequently, a convergent equalizing effect is achieved. To validate the effectiveness of cell-transfer, two experiments are conducted involving two modules, six cells with varying capacities in both non- and equalized discharge. The capacity evolution of modules and intra-module cells with/-out the cell-transfer is shown in Fig. 6, along with the depicted configuration switching actions that exemplify the equalization principle.

The capacity deviation between *M1* and *M2* remains consistent in the non-equalized condition, as depicted in Fig. 6a. Additionally, the cell residual capacities display significant differences when the experiment ends (Fig. 6c). By implementing cell-transfer equalization, the cell *C4* is separated from the stronger *M2* and integrated into *M1* at 200s of the equalized experiment (Fig. 6d: *stage B*). Considering the approximately even distribution of current among intra-module cells, the transfer of *C4* results in a 25% reduction in current flux across *M1*, while the flux passing through *M2* is increased to 1.25×. Consequently, a noteworthy portion of the discharge load is seamlessly transferred from the weaker *M1* to the stronger *M2*, leading to a gradual convergence of module capacities (Fig. 6b). From a cellular perspective, the capacity drops of the *C5* and *C6* in *M2* are accelerated, while the charge consumption on *C1-C4* decelerates starting from 200s. Once the additional 0.9Ah capacity of *M2* is released and both modules reach 2.88Ah at 1134s, the cell-transfer concludes and the *C4* cell returns to *M2* (*stage C* in Fig. 6d). Subsequently, the two modules remain equalized until the experiment ends.

2) Collaborative Splitting Equalization:

In scenarios where two strong modules are adjacent, collaborative splitting demonstrates greater superiority compared to cell-transfer equalization. In this approach, both strong modules are split, and the split-out cells form a new interim module. To affirm the effectiveness of collaborative splitting equalization, two experiments are conducted on a 3P-3S battery, and the corresponding experimental outcomes are presented in Fig. 7.

As depicted in Fig. 7a, the capacity differences remain relatively unchanged until the non-equalized experiment concludes. The substantial gap in module capacities in Fig. 7c indicates poor utilization of pack capacity, with 0.9Ah and 1.05Ah wasted in modules *M2* and *M3*, respectively. On the other hand, the effectiveness of collaborative splitting becomes apparent from 200s in the second experiment. As shown in Fig. 7d, the highest-capacity cells of *M2* and *M3*, *C6* and *C7*, are split and connected to form a new module between *M2* and *M3*. This action significantly increases the discharge flux of *M2* and *M3* to approximately 1.5× of the previous condition. Consequently, the capacity decrease of *M2*, *M3*, and the corresponding cells is accelerated, as evident in Fig. 7b. Once the additional 0.9Ah capacity of *M2* relative to *M1* is consumed at 1217s, *C6* and *C7* return to original modules, and the dual-module splitting concludes. A comparison of Fig. 7c and *stage D* in Fig. 7d clearly

This article has been accepted for publication in IEEE Transactions on Transportation Electrification. This is the author's version which has not been fully edited and content may change prior to final publication. Citation information: DOI 10.1109/TTE.2024.3399218

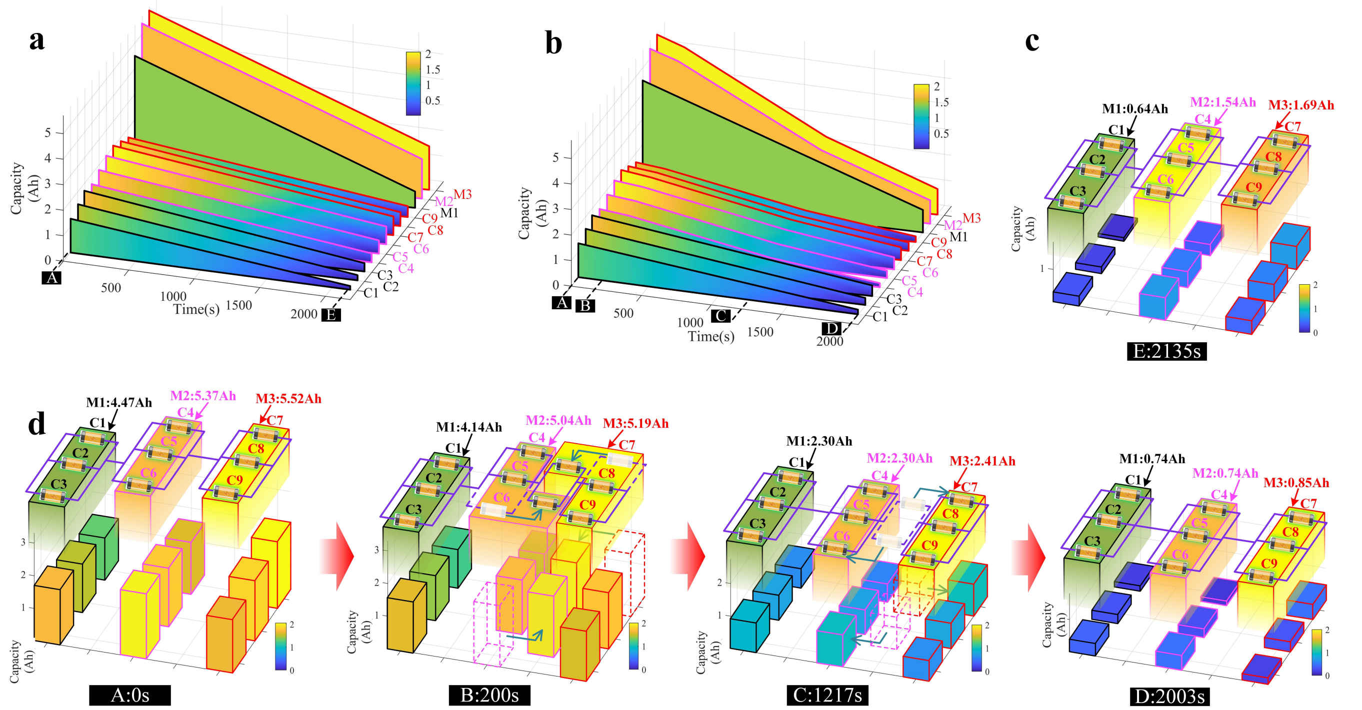

Fig. 7. Capacity of cells and modules: a) without, and b) with the collaborative splitting equalization, where the color gradient indicates the amount of cell residual capacity. c) Module capacity and intra-module cell capacity at the end of non-equalized discharge. d) The collaborative splitting equalization interpreted by configuration switching actions in 4 stages: *A* is the start, *B* is the collaborative-splitting stage, *C* is the dual-module recombination stage, and *D* is the end of equalization.

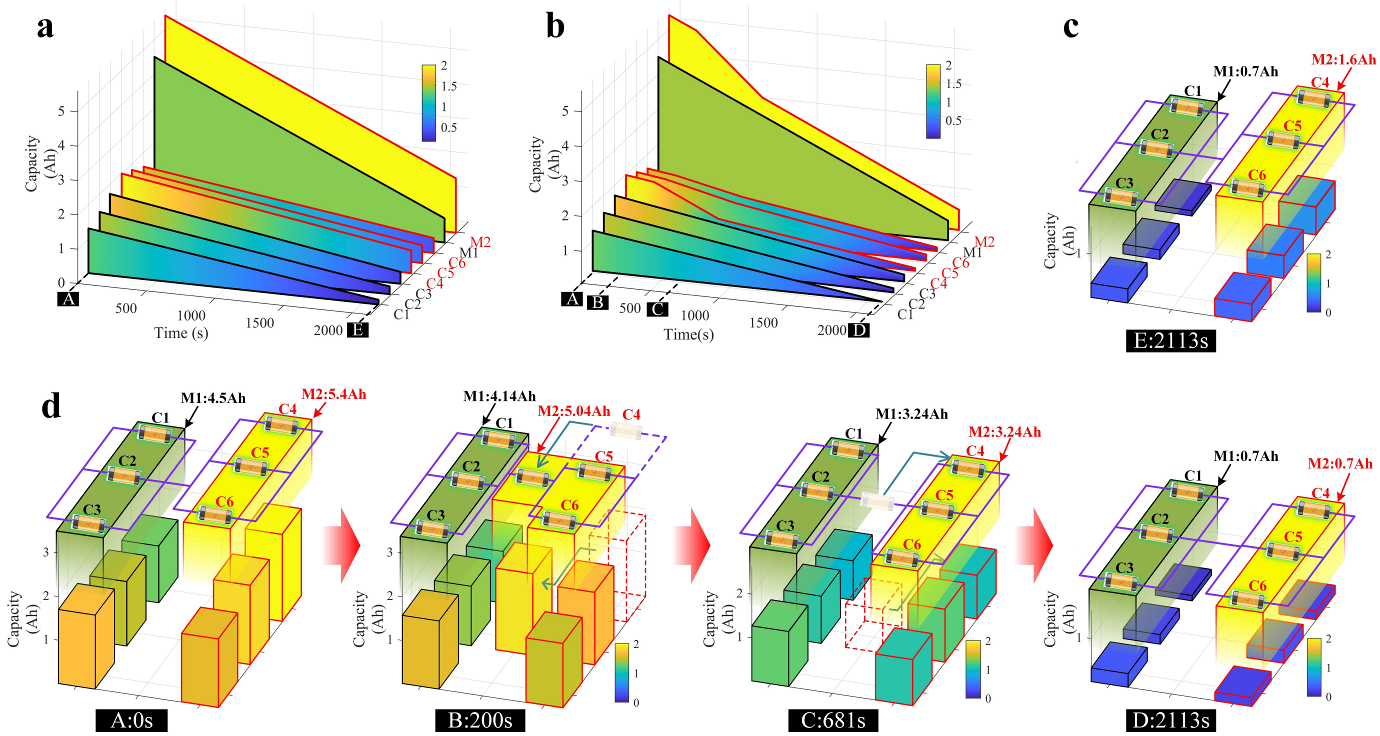

Fig. 8. Capacity of cells and modules: a) without, and b) with the strong-module splitting, where the color gradient indicates the amount of cell residual capacity. c) Module capacity and intra-module cell capacity at the end of non-equalized discharge. d) The strong-module splitting equalization interpreted by configuration switching in 4 stages: *A* is the start, *B* is the strong-module splitting stage, *C* represents the module-recombination stage, and *D* is the end of equalized discharge.

shows that the inconsistency among cells has been significantly reduced by collaborative splitting equalization, representing a substantial improvement compared to the non-equalized case. It can be seen that the pack operating time is reduced from 2135s to 2003s with the implementation of collaborative. The reason is that *C4* in *M2* reaches the discharge termination prematurely due to the excessive discharge by the *M2* splitting. This phenomenon can be effectively addressed when implementing the intra-module cell equalization.

3) Strong-module Splitting Equalization:

The strong-module splitting equalization is suitable for the situations in which the strong and equalized modules are adjacent. In these cases, the strong module is divided into two sub-modules in series, resulting in the split module carrying double flux compared to other modules. When the additional capacity of the strong module is utilized, the split-out cells return and the split module recombines. The same six cells used in the cell-transfer equalization case are employed again to validate the strong-module splitting controller. The changes in module and cell capacity with/-out the strong-module splitting equalization are depicted in Fig. 8, as well as the configuration-switching actions focused on equalization at various stages.

Again, Fig. 8c shows that the initial capacity difference of 0.9Ah between *M1* and *M2* is reserved to the end of discharge without equalization. An evident uneven distribution of residual capacities within *M1* and *M2* is observed. In contrast, when the strong-module splitting equalization takes effect around 200s in the second experiment, the capacity of the stronger *M2* decreases faster. This is due to the split of the cell *C4* from *M2* through switch actions. As a result, the strong *M2* is divided into two sub-modules and discharges at a double rate compared to *M1*. The capacity of *C4* rapidly drops as it carries the current originally shared by three cells. When a discharge flux of 0.9Ah flows through all modules at 681s, the capacity of un-split *M1* reduces by 0.9Ah while *M2* releases 1.8Ah. At this point, the capacity gap between *M1* and *M2* is completely compensated, and the split-out *C4* returns to *M2*. Subsequently, it is observed that the capacities of both modules decrease synchronously to the defined threshold of 0.7Ah. Comparing Fig. 8c and 8d, it is further evident that the differences in cell capacities are almost eliminated at the end of equalization. These results highlight the role of strong-module splitting in eliminating module capacity gaps and mitigating cell capacity inconsistencies.

C. Validation with Battery Pack

The proposed multi-scale reconfiguration control method is implemented on a reconfigurable battery pack with 3P-5S design, which better represents practical scenarios. The experimental results with/-out the proposed method are depicted in Fig. 9. Without utilizing the proposed method, as seen in Fig. 9a and 9c, the capacity inconsistencies of cells and modules remain unchanged, resulting in a significant amount of unutilized capacity. Additionally, the pack voltage is uncontrollable. As shown in Fig. 9e, the pack voltage falls outside the allowable boundary, and the voltage deficit cannot be restored due to the fixed battery configuration. This inevitably hampers the efficiency of the DC/DC and obstructs the efficient transfer of battery charge.

Referring to the results shown in Fig. 9b, 9d, and 9f, it is evident that the battery behaviors change at different stages. From 0 to 1508s, module equalization and intra-module cell equalization are conducted successively. The early period from 0 to 1508s is zoomed in and illustrated in Fig. 9g and 9h. It can be observed that three forms of inter-module equalization are conducted either simultaneously or in an orderly manner to ensure

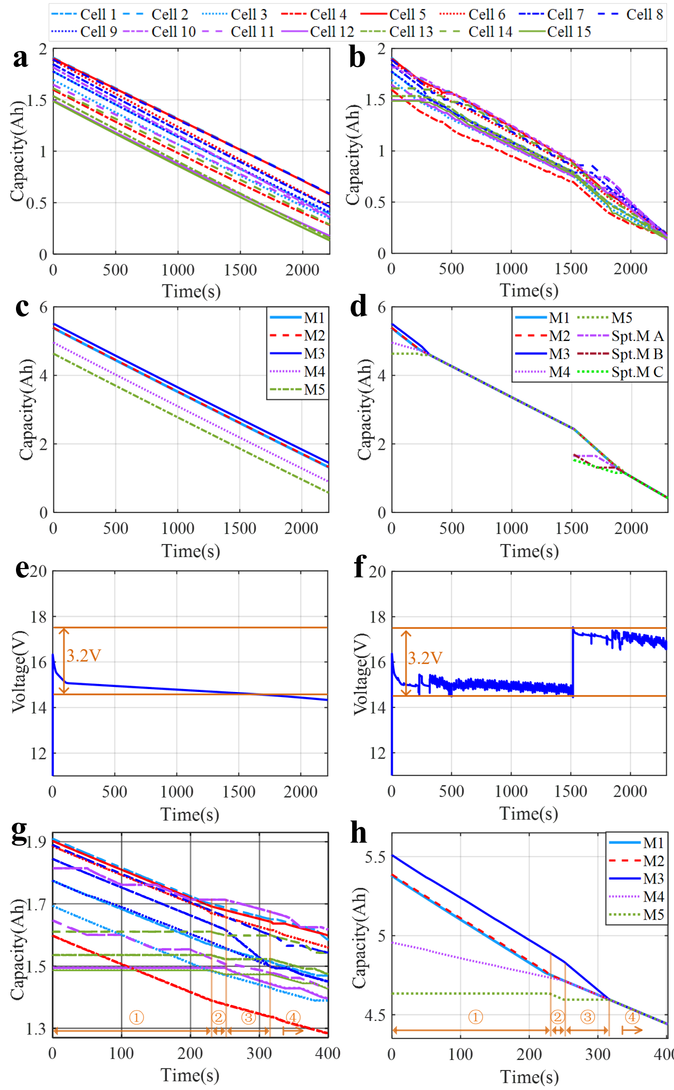

Fig. 9. Experimental results with/-out the multi-scale reconfiguration. a) Cell capacities, c) module capacities, and e) pack voltage when the propose method is absent. b) Cell capacities, d) module capacities, and f) pack voltage under the multi-scale reconfiguration control. g) Zoom-in cell capacities, and h) zoom-in module capacities in the early-stage of 0-1508s in the multi-scale reconfiguration discharge.

the rapid equalization of all modules. Based on the enabling sequence of the module-equalization form, this period can be further divided into *Stage 1-3*.

Correspondingly, the configuration changes at each stage are illustrated in Fig. 10. At *Stage 1*, the collaborative splitting and cell-transfer equalization collaborate to utilize the excess capacities of strong modules *M1*, *M2*, and *M3*. Simultaneously, the weak module exit-return mechanism enables, removing the weak module *M5* to offset the increase in the number of series modules resulting from collaborative splitting. In *Stage 2*, cell-transfer between *M3* and *M4* is conducted exclusively, as the original strong modules *M1* and *M2* have been equalized by the end of *Stage 1*. The weak module *M5* returns as the additional intermediate module of *Cell 3* and *4* by collaborative splitting disappears. Once the excess capacity of *M3*, relative to the average module capacity, is discharged, *Stage 2* transitions to *Stage 3* for strong-module equalization, as there is no suitable adjacent condition for other module equalization modes. When all modules are equalized at 317s, inter-module equalization concludes, and intra-module equalization commences, corresponding to *Stage 4* in Fig. 10. It is observed that the available capacities of the modules consistently decrease under the control of the intra-module equalization controller.

When the pack voltage reaches the lower limit at 1508s, the voltage stabilization control is activated. Specifically, the two strong modules *M3* and *M4* are split collaboratively to form three new modules, *Spt. M A*, *B*, and *C*, as depicted in Fig. 10. This results in an increase of 3.2V in the pack voltage, as shown in Fig. 9f, effectively preventing the occurrence of an uncontrollable voltage gap and ensuring a high DC/DC efficiency. However, the voltage stabilization disrupts the previously equalized state prior to 1508s. Consequently, both inter- and intra-module equalization are consecutively carried out again to find a new equalization for both modules and intra-module cells. As depicted in Fig. 9b and 9d, the equalization of modules and cells is successfully achieved at 1936s and 2302s, respectively.

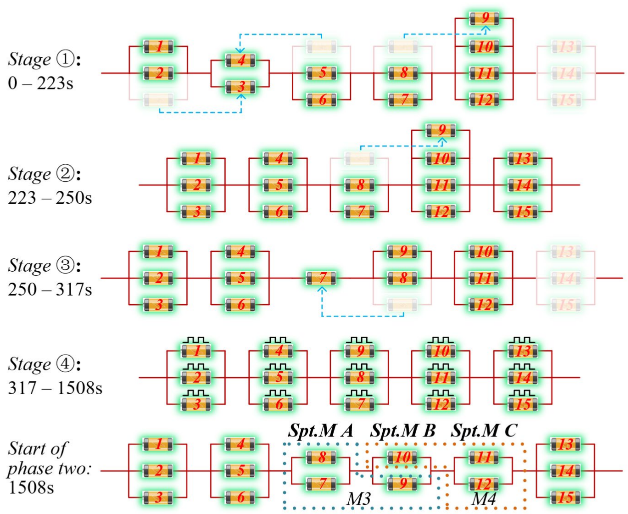

Fig. 10. Pack configurations corresponding to different stages marked in Fig. 9 g) and h).

TABLE VI
Performance of battery pack with/-out the proposed method.

	Available capacity	Capacity utilizing rate	DC/DC efficiency	Efficiency rise
Benchmark	20.28Ah	78.39%	94.62%	-
Proposed method	23.11Ah	89.33%	97.13%	14.34%

The capacity and energy utilization of the 3P-5S pack are measured and summarized in Table VI. The capacity utilization rate observed with the proposed method shows an increase of approximately 11%, while the battery pack efficiency improves by 14.34%. The experiment sets the lower threshold of SOC at 10%, theoretically allowing for a maximum capacity utilization ratio of 90%. Remarkably, the proposed method brings the pack very close to this theoretical upper limit, ensuring high-efficiency operation of the battery system.

The BMS used in the experiment is developed based on the MPC5744P core control unit. The compiled reconfiguration algorithm has a target machine code size of only 52kB, significantly smaller than the memory of the MPC5744P. The average calculation load rate for executing the algorithm is 9.35%. Therefore, the computational complexity of the multi-scale reconfiguration can be comfortably handled by the BMS.

To further validate the effectiveness and scalability of the proposed method, an additional set of 20 experiments is conducted, focusing on the multi-scale reconfiguration control using the 3P-5S reconfigurable prototype. In each experiment, 15 cells are randomly selected from a pool of 50 second-life cells with varying aging states to constitute the battery pack. These battery packs are distinguished by different levels of cell and module capacity differences. The statistical analysis of all 20 experimental results is shown in TABLE VII. It can be seen that that with the increase of cell or module capacity differences, the capacity utilization and DC/DC efficiency of the pack both decrease. However, when reconfiguration control is enabled, the average capacity utilization is increased by more than 10%, and the average DC/DC efficiency is improved by approximately 3%. The statistical results demonstrate the effectiveness of the proposed method, which can significantly improve the capacity utilization and energy conversion efficiency of the battery pack.

TABLE VII
Statistical analysis of 20 multi-scale reconfiguration experiments.

Capacity difference range		Average capacity utilizing rate without Rcf.	**Average capacity utilizing rate with Rcf.**	Average DC/DC Eff. without Rcf.	**Average DC/DC Eff. with Rcf.**
Cell	10% ~ 15%	79.10%	89.24%	94.43%	97.50%
	15% ~ 20%	77.70%	88.76%	94.55%	97.35%
	20% ~ 25%	75.95%	88.39%	93.92%	97.07%
Module	5% ~ 10%	79.09%	89.25%	94.32%	97.41%
	10% ~ 15%	78.13%	88.91%	94.57%	97.36%
	15% ~ 20%	76.62%	88.53%	94.11%	97.22%

D. Validation of Control Robustness

It is important to note that all of the experiments described above are conducted at a temperature of 25°C. To further assess the robustness of the multi-scale reconfiguration, the equalization performance of a 3P-5S reconfigurable battery pack under varying battery temperatures is evaluated.

Firstly, the performance of the multi-scale reconfiguration with fixed cell parameters is examined. Fig. 11(a) shows the evolution of cell capacity when the cell parameters at 25°C are used as inputs for reconfiguration control in an experimental environment at 10°C. It can be observed that without the temperature adaptive parameter update, achieving the goal of equalizing all in-pack cells is difficult. Although the cell capacities show a convergence trend during the experiment, they diverge significantly towards the end at 2163s, indicating poor equalization performance and inadequate capacity utilization.

In contrast, when the parameter update mechanism is enabled, i.e., using the real cell parameters at 10°C as inputs for reconfiguration-based battery multi-scale control at 10°C, the cell capacity evolution depicted in Fig. 11(b) is significantly

This article has been accepted for publication in IEEE Transactions on Transportation Electrification. This is the author's version which has not been fully edited and content may change prior to final publication. Citation information: DOI 10.1109/TTE.2024.3399218

improved. The load supporting time is extended from 2163s to 2210s, indicating the release of more pack capacity. Furthermore, all cell capacities almost converge at the same point by the end of the experiment, indicating successful achievement of equalization among all cells. Statistical analysis shows that the pack capacity utilization in the parameter-update reconfiguration is 88.67%, which is close to the theoretical upper limit. In conclusion, the parameter adaptive update of the multi-scale reconfiguration control ensures its scalability and robustness in the face of changing operating conditions.

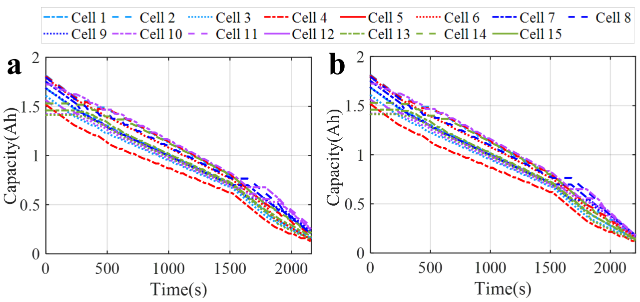

Fig. 11. Experimental results of cell capacity evolution in multi-scale reconfiguration (a) without (b) with temperature adaptive cell parameter updates.

E. Validation with Large-scale Battery Systems

The proposed multi-scale reconfiguration control is further applied to a large-scale battery system to demonstrate its effectiveness and applicability. For the purpose of easy and rapid implementation, the hardware-in-the-loop (HIL) experimental validation is adopted. A battery pack consisting of 444 $LiFePO_4$ battery cells in a 37P-12S configuration is employed, which is a representative number of cells adopted in the commercial Tesla Model S. The cell capacities are distributed within [2.594Ah, 3.390 Ah], reflecting a high capacity inconsistency typical observed in second-life LIBs. The cell resistances are inconsistent in accordance with the different cell capacities, reflecting the fact that the capacity decreases and the internal resistance increases during the cell aging process.

The validation of reconfigurable voltage stabilization at pack level is omitted here due to the lack of detailed DCDC efficiency information compatible with the employed large-scale battery system. However, as discussed in Section III-B, the essence of voltage stabilization is achieved through module collaborative splitting. If the collaborative splitting is proven to be feasible, the voltage stabilization is expected to be effective.

The capacity evolution of modules and cells in the 444-cell large-scale battery system in three equalization scenarios, i.e., without equalization, under passive balancing, and under multi-scale reconfiguration, is shown in Fig. 12. Without any equalization, as can be seen in Fig. 12a and 12b, the capacity evolution of all modules and cells are nearly parallel. This proves that the imbalance of modules and cells also exist in large-scale battery systems, not just in the laboratory-scale prototype. When traditional passive balancing is implemented, the capacity inconsistency among modules and cells mitigates to a certain extent, as shown in Fig. 12c and 12d. The capacity evolution of modules gradually converge, but there still remains a significant capacity gap when the passive balancing experiment ends.

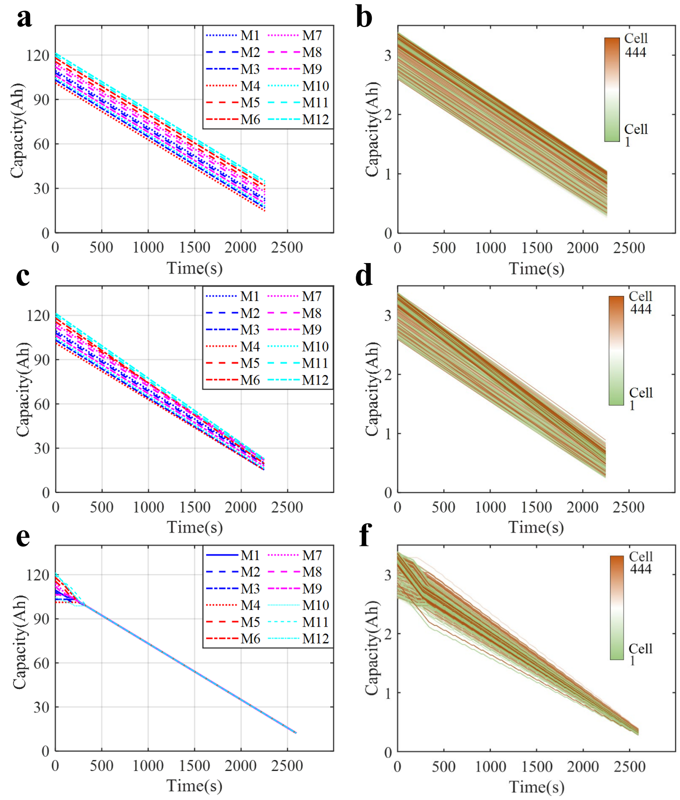

Fig. 12. HIL experimental results for method validation. a), c) and e) Module capacities, b), d) and f) all in-pack cell capacities of free discharge, under passive balancing, and under the proposed multi-scale reconfigurable control method, respectively.

The convergence of cell capacities is even weaker, as passive balancing is only applicable to series modules. Therefore, the cell balancing can only rely on negligible spontaneous balancing of intra-module parallel cells. The proposed multi-scale reconfiguration is then implemented in the same battery system. As can be seen in Fig. 12e and 12f, the capacity difference among modules and cells are almost completely eliminated when the reconfiguration enables. It can be seen that the module equalization is achieved in just 340 seconds by reconfigurable control, demonstrating its significant advantage in balancing speed compared to traditional passive balancing. Although some cells release relatively large capacities in inter-module equalization phase, that is, several cell capacity is outlier from the majority, the capacity of all in-pack 444 cells converges to an extremely narrow range in the end of experiment. It is worth mentioning that the reconfigurable experiment lasts longer than the other two, indicating the elimination of weak cell limitations and the utilization of the large-scale battery system's capacity to its fullest extent in multi-scale reconfigurable control.

TABLE VIII
Performance of large-scale battery system in different method.

	Available capacity	Capacity utilizing rate	Capacity utilizing rise
Benchmark	1037.93Ah	77.82%	-
Passive balancing	1099.95Ah	82.47%	4.65%
Proposed method	1187.18Ah	89.01%	11.19%

The capacity utilization of the 444-cell large-scale battery pack under different equalization scenarios is measured and summarized in TABLE VIII. It can be seen that the capacity utilization of the large-scale battery pack under reconfigurable control approach its maximum capacity utilization ratio of 90%. Compared to unbalanced situation, passive balancing increased the pack capacity utilization by 4.65%, while the proposed multi-scale reconfigurable control achieved a capacity utilization improvement of 11.19%.

All above phenomenon clearly indicate that the proposed multi-scale reconfigurable method can achieve maximum capacity utilization and higher energy conversion efficiency in large-scale battery systems, superior to widely adopted passive balancing methods.

The reconfiguration HIL experiment of large-scale battery system also adopts the MPC5744P-based BMS controller. With an average calculated load rate of 38.74% during the experiment, it can be inferred that the proposed multi-scale reconfiguration control approach possesses low computational complexity and presents a highly feasible solution for optimizing the operation of large battery packs.

The recent concerns regarding the safety of using second-life batteries in large-scale grid energy storage are valid. This is primarily due to the limitations of static-connected retired batteries, which fail to address capacity disparities among individual cells and are thus susceptible to issues such as overcharging and discharging of weaker cells. In response to these challenges, the multi-scale reconfigurable control method proposed in this paper offers a potential solution by ensuring equalization of all cells within the battery pack. This approach significantly enhances the fault tolerance and overall safety of second-life battery systems comprising highly inconsistent cells. Moving forward, the demonstration application of reconfigurable second-life batteries in small-scale scenarios like home energy storage systems, communication base station energy storage, and low-power electric vehicles can serve as a basis for gradually expanding their application in large-scale grid energy storage.

V. Conclusions

Based on a 4-switch reconfigurable battery topology, a multi-scale reconfiguration control method is proposed to mitigate the significant cell inconsistency that arises during second-life usage of batteries. To validate the effectiveness of the proposed method, a laboratory-scale prototype of the reconfigurable battery pack with the proposed controller is constructed. The major conclusions are summarized as follows:

(1) The 4-switch topology ensures all-cell flexibility. The multi-scale reconfiguration promises all-cell equalization. With the proposed method, the deviation of cell residual capacities in a highly-imbalanced pack can be confined to 54.5mAh, equivalent to state-of-charge inconsistency of only 1.26%.

(2) The pack voltage can be stabilized within a defined range by using the proposed method. The regulation resolution equals to the single-cell voltage, which is refined enough considering the high pack voltage in practical applications.

(3) The capacity inconsistency of second-life batteries can be compensated efficiently by using the proposed method, i.e., the capacity utilization is elevated by 10.96%, approximating the theoretical upper limit of total capacity of pack. Meanwhile, the pack efficiency can be improved largely by 14.34%.

Considering that the large capacity inconsistency among cells challenges the efficient and safe post-vehicle applications, the proposed method can provide an insightful solution for the management of the second-life battery systems.

The application scope of the multi-scale reconfiguration control is not restricted to the employed 4-switch reconfigurable topology, but can be partially or completely extended to other topologies that support intra-module cell independence and intra-module configuration changes. In the future, the feasibility of the multi-scale reconfiguration control in other topologies will be explored. In addition, it is important to consider the potential risk of battery system failures when introducing a large number of switches in reconfigurable topologies. Therefore, the detailed reconfiguration-based fault-tolerant control is also an important topic in the research future.

References

[1] W. Li, Q. Du, G. Guo *et al.*, “Enhanced electrochemical and thermal behavior of lithium-ion batteries with ultrathick electrodes via oriented pores,” *Applied Thermal Engineering,* vol. 228, pp. 120555, 2023.

[2] E. Galiounas, T. G. Tranter, R. E. Owen *et al.*, “Battery state-of-charge estimation using machine learning analysis of ultrasonic signatures,” *Energy and AI,* vol. 10, pp. 100188, 2022.

[3] H. Ruan, J. Chen, W. Ai *et al.*, “Generalised diagnostic framework for rapid battery degradation quantification with deep learning,” *Energy and AI,* vol. 9, pp. 100158, 2022.

[4] K. Zhang, R. Xiong, S. Qu *et al.*, “Electrochemical Impedance Spectroscopy: A Novel High-Power Measurement Technique for Onboard Batteries Using Full-Bridge Conversion,” *IEEE Transactions on Transportation Electrification*, 2024.

[5] X. Lai, Y. Huang, H. Gu *et al.*, “Turning waste into wealth: A systematic review on echelon utilization and material recycling of retired lithium-ion batteries,” *Energy Storage Materials,* vol. 40, pp. 96-123, 2021.

[6] Z. Xu, J. Wang, P. D. Lund *et al.*, “A novel clustering algorithm for grouping and cascade utilization of retired Li-ion batteries,” *Journal of Energy Storage,* vol. 29, pp. 101303, 2020.

[7] K. Rumpf, A. Rheinfeld, M. Schindler *et al.*, “Influence of cell-to-cell variations on the inhomogeneity of lithium-ion battery modules,” *Journal of The Electrochemical Society,* vol. 165, no. 11, pp. A2587, 2018.

[8] S. Narayanaswamy, S. Steinhorst, M. Lukasiewycz *et al.*, “Optimal dimensioning and control of active cell balancing architectures,” *IEEE Transactions on Vehicular Technology,* vol. 68, no. 10, pp. 9632-9646, 2019.

[9] Q. Ouyang, J. Chen, J. Zheng *et al.*, “Optimal cell-to-cell balancing topology design for serially connected lithium-ion battery packs,” *IEEE transactions on sustainable energy,* vol. 9, no. 1, pp. 350-360, 2017.

[10] M. Caspar, T. Eiler, and S. Hohmann, “Systematic comparison of active balancing: A model-based quantitative analysis,” *IEEE transactions on vehicular technology,* vol. 67, no. 2, pp. 920-934, 2016.

[11] R. de Castro, C. Pinto, J. V. Barreras *et al.*, “Smart and hybrid balancing system: Design, modeling, and experimental demonstration,” *IEEE Transactions on Vehicular Technology,* vol. 68, no. 12, pp. 11449-11461, 2019.

[12] F. Feng, X. Hu, J. Liu *et al.*, “A review of equalization strategies for series battery packs: variables, objectives, and algorithms,” *Renewable and Sustainable Energy Reviews,* vol. 116, pp. 109464, 2019.

[13] D. Andrea, "Battery management systems for large lithium-ion battery packs," Artech house, 2010.

[14] W. Huang, and J. A. A. Qahouq, “Energy sharing control scheme for state-of-charge balancing of distributed battery energy storage system,” *IEEE Transactions on Industrial Electronics,* vol. 62, no. 5, pp. 2764-2776, 2014.

[15] M. Einhorn, W. Guertlschmid, T. Blochberger *et al.*, “A current equalization method for serially connected battery cells using a single

power converter for each cell," *IEEE Transactions on Vehicular Technology,* vol. 60, no. 9, pp. 4227-4237, 2011.
[16] Z. Wei, J. Zhao, H. He *et al.*, "Future smart battery and management: Advanced sensing from external to embedded multi-dimensional measurement," *Journal of Power Sources,* vol. 489, pp. 229462, 2021.
[17] N. Bouchhima, M. Schnierle, S. Schulte *et al.*, "Optimal energy management strategy for self-reconfigurable batteries," *Energy,* vol. 122, pp. 560-569, 2017.
[18] N. Bouchhima, M. Gossen, S. Schulte *et al.*, "Lifetime of self-reconfigurable batteries compared with conventional batteries," *Journal of Energy Storage,* vol. 15, pp. 400-407, 2018.
[19] F. Ji, L. Liao, T. Wu *et al.*, "Self-reconfiguration batteries with stable voltage during the full cycle without the DC-DC converter," *Journal of Energy Storage,* vol. 28, pp. 101213, 2020.
[20] L. He, E. Kim, and K. G. Shin, "A case study on improving capacity delivery of battery packs via reconfiguration," *ACM Transactions on Cyber-Physical Systems,* vol. 1, no. 2, pp. 1-23, 2017.
[21] N. Bouchhima, M. Schnierle, S. Schulte *et al.*, "Active model-based balancing strategy for self-reconfigurable batteries," *Journal of Power Sources,* vol. 322, pp. 129-137, 2016.
[22] S. Ci, J. Zhang, H. Sharif *et al.*, "Dynamic reconfigurable multi-cell battery: A novel approach to improve battery performance." pp. 439-442.
[23] T. Kim, W. Qiao, and L. Qu, "A series-connected self-reconfigurable multicell battery capable of safe and effective charging/discharging and balancing operations." pp. 2259-2264.
[24] A. Manenti, A. Abba, A. Merati *et al.*, "A new BMS architecture based on cell redundancy," *IEEE Transactions on Industrial Electronics,* vol. 58, no. 9, pp. 4314-4322, 2010.
[25] T. Kim, W. Qiao, and L. Qu, "Power electronics-enabled self-X multicell batteries: A design toward smart batteries," *IEEE Transactions on Power Electronics,* vol. 27, no. 11, pp. 4723-4733, 2012.
[26] X. Wang, B. Duan, Y. Shang *et al.*, "Fast equalization for lithium ion battery packs based on reconfigurable battery structure." pp. 1149-1154.
[27] W. Han, T. Wik, A. Kersten *et al.*, "Next-generation battery management systems: Dynamic reconfiguration," *IEEE Industrial Electronics Magazine,* vol. 14, no. 4, pp. 20-31, 2020.
[28] X. Gong, R. Xiong, and C. C. Mi, "Study of the characteristics of battery packs in electric vehicles with parallel-connected lithium-ion battery cells," *IEEE Transactions on Industry Applications,* vol. 51, no. 2, pp. 1872-1879, 2014.
[29] B. Wang, C. Ji, S. Wang *et al.*, "Study of non-uniform temperature and discharging distribution for lithium-ion battery modules in series and parallel connection," *Applied Thermal Engineering,* vol. 168, pp. 114831, 2020.
[30] W. Han, and A. Kersten, "Analysis and estimation of the maximum circulating current during the parallel operation of reconfigurable battery systems." pp. 229-234.

Zhongbao Wei (Senior Member, IEEE) received the B.Eng. and the M.Sc. degrees in instrumental science and technology from Beihang University, China, in 2010 and 2013, and the Ph.D. degree in power engineering from Nanyang Technological University, Singapore, in 2017.

He has been a research fellow with Energy Research Institute @ NTU, Nanyang Technological University from 2016 to 2018. He is currently a professor in vehicle engineering with the National Engineering Laboratory for Electric Vehicles, Beijing Institute of Technology, China. He has authored more than 100 peer-reviewed articles. His research interests include electrified transportation and battery management. His research interests include electrified transportation and battery management. He serves as Associate Editor for many international journals like IEEE Transactions on Industrial Electronics, IEEE Transactions on Intelligent Transportation Systems, and IEEE Transactions on Transportation Electrification.

Haoyong Cui received the B.Eng. and the M.Sc. in vehicle engineering from Jilin University, Changchun, China, in 2016 and 2019, respectively. He is currently pursuing the Ph.D. degree in mechanical engineering at Beijing Institute of Technology, Beijing, China.

His research interests include the reconfigurable and smart batteries, energy management strategy of hybrid electric vehicles.

Xinghua Liu (Senior Member, IEEE) received the B.S. degree from Jilin University, Changchun, China, in 2009, and the Ph.D. degree in automation from the University of Science and Technology of China, Hefei, China, in 2014.

From 2014 to 2015, he was invited as a Visiting Fellow with RMIT University, Melbourne, VIC, Australia. From 2015 to 2018, he was a Research Fellow with the School of Electrical and Electronic Engineering, Nanyang Technological University, Singapore. He joined the Xi'an University of Technology, Xi'an, China, as a Professor since September 2018. His research interests include state estimation and control, intelligent systems, autonomous vehicles, cyber-physical systems, and robotic systems.

Yang Li (Senior Member, IEEE) received the B.E. degree in electrical engineering from Wuhan University, Wuhan, China, in 2007, and the M.Sc. and Ph.D. degrees in power engineering from Nanyang Technological University (NTU), Singapore, in 2008 and 2015, respectively.

He was a Research Fellow with the Energy Research Institute, NTU, and the School of Electrical Engineering and Computer Science, Queensland University of Technology, Brisbane, QLD, Australia. He joined the School of Automation, Wuhan University of Technology, Wuhan, in 2019, as a Faculty Member. Since 2020, he has been a Researcher with the Department of Electrical Engineering, Chalmers University of Technology, Gothenburg, Sweden. His research interests include modeling and control of energy storage systems in power and transport sectors. Dr. Li serves as an Associate Editor for IEEE Transactions on Transportation Electrification.

Rui Wang (Member, IEEE) received the B.S. degree in electrical engineering and automation and the Ph.D. degree in power electronics and power drive from Northeastern University, Shenyang, China, in 2016 and 2021, respectively, where he is a Lecturer. He has authored or coauthored over 50 papers, authorized over 20 invention patents. His research interest focuses on collaborative optimization of distributed generation and its stability analysis of electromagnetic timescale in cyber-energy system.